Published in final edited form as:
Acta Biomater. 2012 July ; 8(7): 2456–2465. doi:10.1016/j.actbio.2012.03.026.

Mineralization of Peptide Amphiphiles Nanofibers and its Effect on Differentiation of Human Mesenchymal Stem Cells

Timothy D. Sargeant,
Department of Materials Science and Engineering, Northwestern University, 2220 Campus Drive, Evanston, IL 60208-3108 (USA)

Conrado Aparicio,
Institute for Bionanotechnology for Medicine, Northwestern University, 303 E. Superior, Chicago, IL 60611-2875 (USA), Biomaterials and Biomechanics Division, Department of Materials Science, Universitat Politècnica de Catalunya, Av. Diagonal 647, 08028, Barcelona, Spain

Josh Goldberger,
Department of Chemistry, Northwestern University, 2220 Campus Drive, Evanston, IL 60208-3108 (USA)

Honggang Cui, and
Department of Materials Science and Engineering, Northwestern University, 2220 Campus Drive, Evanston, IL 60208-3108 (USA)

Samuel I. Stupp
Department of Materials Science and Engineering, Department of Chemistry, Department of Medicine, Institute for Bionanotechnology for Medicine, Northwestern University, 2220 Campus Drive, Evanston, IL 60208-3108 (USA), Phone: (+1) 312-503-0807, Fax: (+1) 847-491-3010

Samuel I. Stupp: s-stupp@northwestern.edu

Abstract

One of the important targets in regenerative medicine is to design resorbable materials that can promote formation of new bone in large skeletal defects. One approach to this challenge is to use a bioactive and biodegradable organic matrix that can promote cellular adhesion and direct differentiation. We studied here matrices composed of peptide amphiphiles (PAs) that self-assemble into nanofibers and create self-supporting gels in cell culture conditions. The bioactivity of PAs was designed by incorporating in their peptide sequences phosphoserine residues to promote hydroxyapatite formation in the culture medium and the cell adhesion epitope RGDS. In calcium supplemented osteogenic media, the PA nanofibers were found to nucleate spheroidal nanoparticles approximately 100 nm in diameter of crystalline carbonated hydroxyapatite. This mineralization mode is not epitaxial relative to the long axis of nanofibers and occurs in the presence of serine or phosphoserine residues in the peptide sequence of the amphiphiles. Mixing of the phosphoserine-containing PAs with 5 weight % of RGDS-containing PA molecules does not inhibit formation of the mineral nanoparticles. Quantitative real-time reverse transcription polymerase chain reaction (QRT-PCR) and immunohistochemistry (IHC) analysis for alkaline phosphatase (ALP) and osteopontin expression suggest that these mineralized matrices promote

Correspondence to: Samuel I. Stupp, s-stupp@northwestern.edu.

osteogenic differentiation of human mesenchymal stem cells. Based on ALP expression, the presence of phosphoserine residues in PA nanofibers seem to benefit osteogenic differentiation.

Keywords

regenerative medicine; tissue engineering; self-assembly; bone; phosphoserine; human mesenchymal stem cell; calcium phosphate; hydroxyapatite

1. Introduction

The current gold standard for bone replacement is an autologous graft harvested from the iliac crest [1–3]. The problematic issues with autografts include defect size limits, complications with donor site morbidity, and pain. Alternatives include the use of allografts and a variety of bioceramics [4]. These alternatives also have considerable limitations, including limited number of donors and high cost for allografts, and poor mechanical properties and integration for ceramics. Therefore, there is significant need to create bioactive materials that could effectively fill bone defects and be fully resorbable as they promote bone regeneration. There has been an extensive amount of work on biomimetic materials in the context of mineralization that could be considered to develop our vision for bone replacement [5].

Our laboratory has been interested for over a decade in the molecular design of biomimetic and biodegradable matrices that can promote bone formation. We reported earlier on materials known as organoapatites [6–10] and our more recent focus has been on a class of materials known as peptide amphiphiles (PAs) [11–15]. The PAs are broadly suitable for regenerative medicine since their bioactivity can be molecularly tailored. Previous work by our laboratory [11] demonstrated the templated formation of hydroxyapatite on PA nanofibers bearing phosphorylated serine (S(P)) residues, which mimics the high occurrence of these amino acids in phosphophoryn, an important protein in the formation of dentin[16]. There has also been interest in developing mixed systems of PAs, allowing for the molecular control of epitopes presented on the exterior of the nanofiber surface. In this work we were interested in incorporating PA nanofibers containing the biological adhesion epitope Arg-Gly-Asp-Ser (RGDS) at controlled concentrations in addition to phosphorylated serine residues to template hydroxyapatite. Indeed, RGDS and other binding domains have been incorporated into peptide amphiphiles as an approach to improve cellular adhesion [17, 18]. Furthermore, our objective in this work has been to probe the response of cells to mineralized PA nanofibers. We probe here the differentiation of human mesenchymal stem cells in contact with the PA nanofiber gels using quantitative real-time reverse transcription polymerase chain reaction (QRT-PCR) in order to probe expression of osteogenic markers. Production of these protein markers was confirmed by immunohistochemistry (IHC). We have also used in this work a number of structural characterization techniques, including scanning electron microscopy (SEM), Fourier-transform infrared (FT-IR) spectroscopy, and transmission electron microscopy (TEM) to characterize mineralization on the PA nanofibers.

2. Materials & Methods

All chemical reagents, unless otherwise noted, were purchased from Sigma-Aldrich (St. Louis, MO). Solvents were purchased from Fisher Scientific (Hanover Park, IL). Amino acids were purchased from EMD Biosciences (San Diego, CA). Human mesenchymal stem cells (hMSCs) and medium components were purchased from Lonza (Switzerland). Other cell culture supplies were purchased from VWR (West Chester, PA).

2.1. Peptide Amphiphile Preparation

Peptide amphiphiles (PA) were synthesized using solid phase peptide synthesis methods previously reported [19, 20], purified by prep-scale high performance liquid chromatography (HPLC), and characterized using electron spray ionization spectroscopy (ESI) and analytical HPLC. Three different PAs were synthesized, a negatively charged PA containing phosphoserine residues (S(P) PA), a negatively charged PA containing serine residues (S PA), and a positively charged PA containing the RGDS sequence (RGDS PA). All three PAs were designed to contain either two lysines or two glutamic acids in their sequences to promote mixing of oppositely charged molecules. The structures of all three PAs are shown in Figure 1. From these three PAs, four different 10 mM PA gel mixtures were prepared: 100% S PA, 95% S/5% RGDS PA, 100% S(P) PA, and 95% S(P)/5% RGDS PA.

2.2. PA Gelation

Dry PA powder was reconstituted in 0.2 μm filtered H_2O to 10 mM concentration and sterilized with UV light for 20 minutes. Osteogenic medium (Lonza) was supplemented with 20 mM $CaCl_2$, hereafter known as mineralization medium. PA scaffolds were created by adding 50 μL of mineralization medium to 50 μL of PA solution in a 96-well plate, which triggered self-assembly of the PA molecules into nanofibers and form a gel. To create pre-mineralized samples, PA gels were incubated at 37 °C and 5% CO_2 *without* cells for 2 weeks.

2.3. Cell Culture

Prior to experiments, human mesenchymal stem cells (hMSCs) were cultured under standard tissue culture conditions at 37 °C and 5% CO_2 in growth medium (Lonza). During the studies, cells were cultured inside PA gels or on top of PA gels at 37 °C and 5% CO_2 in mineralization medium, with half the mineralization medium exchanged for fresh mineralization medium every three days. For experiments with cells on top, PA gels were made as described above, with or without pre-mineralization. A total of 50,000 cells were added to each sample in a small volume, allowed to adhere for 3–4 hours, and then mineralization medium was added for culturing. To create PA gels with encapsulated hMSCs, 50 000 cells were added to the 50 μL of mineralization medium prior to adding it to the PA solution. PA gels were incubated for 30 minutes to allow the gels to set, and then 200 μL of additional mineralization medium was added.

2.4. Biological Analysis

PA gels with cells were assayed by quantitative real-time polymerase chain reaction (QRT-PCR) and immunohistochemical (IHC) staining for two osteogenic markers, alkaline phosphatase (ALP) and osteopontin (OP). For QRT-PCR, samples were cultured for 2 or 4 weeks. Purified RNA was prepared and then reverse transcribed into cDNA using standard protocols. QRT-PCR was then run using a Bio-Rad iCycler Thermal Cycler (Hercules, CA) with Bio-Rad iQ5 software. The following primer sequences were used in PCR experiments:

ALP: Forward ACAACGAGATGCCCCCTGAG

ALP: Reverse CCCCTGGCTTTCTCGTCACT

OPN: Forward GTGATGTCCTCGTCTGTAGCATCA

OPN: Reverse GTAGACACATATGATGGCCGAGG

Reverse transcription was performed using Superscript III (Invitrogen) and a Promega Plexor master mix (Promega). The data were quantified and normalized against GAPDH housekeeping gene (Promega).

For IHC staining, samples were cultured for 4 weeks. Samples were embedded in Tissue-Tek O.C.T. compound (Sakura Finetek USA, Torrance, CA), frozen to −80 °C, and cryo-sectioned using a Microm HM550 microtome. Sections cut to 5 μm thickness were mounted on glass slides and IHC stained using OP or ALP anti-human primary antibodies (R&D Systems, Minneapolis, MN), a streptavidin HRP mouse bioassay IHC kit with DAB chromagen (US Biological, Swampscott, MA), and hematoxylin counter stain as per standard protocols. Control samples were prepared using the same protocol, without the addition of the primary antibody.

2.5. Mineral Characterization

PA gels for mineralization characterization were prepared as described above without cells and cultured for various times in mineralization medium at 37 °C and 5% CO_2, with 50% medium exchanges every 3 days. Mineralization of the PA gels was characterized by scanning electron microscopy (SEM), Fourier transform infrared spectroscopy (FT-IR), and transmission electron microscopy (TEM).

SEM samples were removed from culture and dehydrated in graded ethanol solutions up to 100% ethanol, followed by critical point drying. Samples were then coated with 3 nm Au-Pd and imaged on an FEI Quanta ESEM fitted with a Schottky thermal field emission gun and Oxford EDS at 10kV. A secondary electron detector was used for high-resolution imaging.

FT-IR samples were removed from media after 14 days of culture and gently rinsed with PBS and ultrapure water. They were dried in a desiccator under vacuum for at least 24 h. Samples included non-mineralized PA, mineralized PA, and mineralized PA that was burned in an oven for 5 h at 250 °C, 350 °C, 450 °C or 550 °C. Samples were prepared as a KBr-pellet and analyzed with a Thermo Nicolet, Nexus 870 FT-IR with the Tabletop Optics Module (TOM) over the range 4000-400 cm^{-1} at 0.4 cm^{-1} resolution averaging 128 scans.

TEM samples were prepared by two different methods. First, samples were removed from medium, rinsed in ultrapure H_2O, and burned at 350 °C. The remaining mineral was collected and placed onto a holey carbon coated Cu TEM grids. Images, diffraction patterns, and EDS spectra were obtained using a JEOL JEM-2100F FAST TEM equipped with a high-brightness Schottky FEG emitter operated at 200kV. Alternatively, a second set of samples were removed from culture, fixed in 2% gluteraldehyde and 2% paraformaldehyde, rinsed in PBS, post-fixed in 1% OsO_4, and rinsed in PBS. Samples were then dehydrated in graded acetone and embedded in EmBed-812/DER 73 (Electron Microscopy Sciences) according to protocol. Briefly, samples were soaked in a 1:2 solution of EMbed-812/DER 73 and acetone, a 1:1 solution of EMbed-812/DER 73 and acetone, and then straight EMbed-812/DER 73 with several fresh exchanges. The resin was then cured for 24 hours at 60 °C. Samples were then section to approximately 70 nm thick using a glass knife, and floated onto a Cu TEM grid. Lastly, another subset of the samples was stained with uranyl acetate before imaging on a JEOL 1230 TEM equipped with a Hamamatsu ORCA camera and AMT imaging software at 100 kV.

2.6. Statistics

Multivariate analysis was performed with JMP 6 software to determine significance values (α-value) and power values (P-value). For individual comparisons, T-test with unknown variance was used to determine two-tailed P-values. Significance was set at $\alpha = 0.05$. Statistics for biological analysis are shown using 95% confidence error bars.

3. Results and Discussion

3.1. Mineralization of Peptide Amphiphile Nanofibers

Peptide amphiphile gels were prepared without cells and incubated with mineralization medium at 37 °C and 5% CO_2 to study the evolution of mineral growth. As shown in Figure 2, SEM imaging from day 3 shows the formation of spherical mineral that is associated only with the nanofibers for all samples. The mineral has a spherical morphology with dimensions on the order of 100 nm in diameter for all samples after 3 days of incubation in osteogenic medium. After 7 days of mineral growth, the spheres still typically measure 100 nm in diameter, but grow denser along the nanofibers with time. At higher magnification (Figure 3), it is clear that the mineral is associated with the nanofibers, indicating the mineral is templating from the PA and is not the result of aqueous precipitation. Additionally, the high resolution image confirms the mineral is spherical and not an agglomerate of nanocrystals. This morphological observation is important, and will be discussed later in the manuscript. To better characterize the mineral on the PA nanofibers, samples were prepared for analysis by FT-IR spectroscopy and TEM. Mineralized PA gels were first washed repeatedly with distilled H_2O to remove residual medium components, including salts that might have precipitated during sample preparation. PA gels were then heated to increasing elevated temperatures to remove the organic (PA and medium) components. FT-IR spectra of mineralized S(P) and S PA gels before and after heating at elevated temperatures are shown in Figure 4. Spectra for both of the unheated PA samples show contributions from PA and mineral. Several bands are observed that correspond to the amines in the PA structure, including 1635–1670 cm^{-1} (amide I), 1545 cm^{-1} (amide II), and 1400 and 1445 cm^{-1} (amide III), respectively. The amide I band is bimodal, and indicates the contribution of β-sheet and α-helix conformations (1635 cm^{-1} and 1670 cm^{-1}, respectively) in the nanofiber structure [11]. Additional bands are observed in FTIR spectra corresponding to the mineral, including HPO_4^{2-} (1090–1100 cm^{-1}), υ_3 PO_4^{3-} (1045, 603, and 570 cm^{-1}), υ_1 PO_4^{3-} (960 cm^{-1}), and B-type CO_3^{2-} (875–878 cm^{-1}). When the PA is heated to increasing elevated temperatures, the bands contributed by the PA nanofibers are reduced, and are not present in the 350 °C spectrum. This indicates that the PA is being burned off, leaving the mineral behind. As the amide III bands (1400 and 1445 cm^{-1}) disappear, a new bimodal band emerges (1420–1430 and 1470–1480 cm^{-1}), corresponding to B-type CO_3^{2-}. Combined, this indicates that the mineral formed on S(P) PA and S PA is the same, and is a carbonated, slightly calcium-deficient, crystalline hydroxyapatite. Indeed, naturally occurring hydroxyapatite is typically non-homogenous, non-stoichiometric and contains impurities like carbonate [21]. B-type carbonated apatites have CO_3^{2-}-for-PO_4^{3-} substitutions, and are the primary type found in normal enamel, dentin, and bone [21]. The FT-IR results also indicate that heating the mineralized PA gels at 350 °C is sufficient to remove the organic component, leaving only the mineral behind. While the phosphate absorption bands are broad in the unburned samples, this can be explained by the overlapping of the PA signal and the effect of drying of the nano-sized mineral spheres [22]. Both of these factors would be expected to broaden the bands corresponding to mineral. Additionally, amorphous calcium phosphate is stable beyond 500 °C, and will only begin to convert to poorly crystallized apatite at 600 °C [21]. The only other possible route of conversion, solution-mediated transformations [21], is not a factor in this instance. Therefore, we can conclude that the templated calcium phosphate is indeed crystalline apatite.

To verify the identity of the apatite, additional data was obtained by TEM. Mineralized PA gels were washed and heated to 350 °C, and then analyzed by TEM to obtain images and diffraction patterns, as shown in Figure 5. The TEM images show the agglomerated, unstained mineral formed on S(P) and S PA nanofibers, respectively. Consistent with the FT-IR results above, washing and heating the PA gels to 350 °C removed the organic and

salts components, leaving only the mineral formed on the PA nanofibers. EDS spectra from these samples show strong peaks for calcium, phosphorous, and oxygen, with only trace amounts of other elements. Diffraction patterns obtained were similar in different regions of the sample, and indexing confirms the formation of hydroxyapatite. This confirms the findings by FT-IR, and is consistent with previous mineralization experiments with other phosphoserine-bearing PA systems [11]. Here and in our previous work [11], hydroxyapatite is formed on the PA nanofibers, even though the chemical structures of the PA and the mineralization conditions were quite different, indicating a preference for this particular phase of calcium phosphate in these systems. In the mineralization of S(P)-bearing PA demonstrated by our group previously, mineral was templated on a dried two-dimensional layer of PA nanofibers by immersion at the interface of two solutions containing calcium and phosphate ions, respectively. As a result, the two solutions mixed at the PA nanofiber coating interface in a highly controlled manner. This resulted in epitaxial crystallization of hydroxyapatite on the phosphoserine presenting PA nanofibers. The c-axis of these crystals was parallel to the fiber axis thus yielding a biomimetic structure similar to natural bone where the same orientation occurs relative to collagen fibers. In comparison, the mineralization observed in this work corresponds to bulk mineralization of 3D PA gels cultured in hMSC osteogenic medium under standard culture conditions. Here, we do not see evidence for epitaxial mineralization observed in the two-dimensional system [11] described above and also in different 3D gels with S(P) residues with a different culture medium [12]. In these systems the epitaxial oriented crystals are observed in direct contact with the fibers. Instead we observed here extensive nucleation of spherical hydroxyapatite on PA nanofibers using standard osteogenic hMSC culture conditions. We assume the spherical nature of the mineral indicates its precursor was an amorphous calcium phosphate phase [23]. However, due to the extensive precipitation of mineral in the osteogenic culture medium used here, we cannot rule out the presence of epitaxial mineralization directly on the surface of the nanofibers. Based on our previous work [11, 12], this tends to occur on nanofibers displaying phosphorylated serine residues. However, the difference in this case from our previous work is the use of calcium supplemented osteogenic stem cell medium. This led to the formation of spherical mineral, unlike the templated mineral formed on PA nanofibers exposed to a calcium chloride solution on one side and a sodium phosphate solution on the other [11], or MEM-α medium supplemented with calcium and β-glycerophosphate [12], which slowly releases phosphate ions for mineralization. Also, the mineral precipitation observed here was observed with PA nanofibers with and without the phosphate groups presented in high density on their exterior surfaces. The extensive mineralization with spherical particles observed in the osteogenic medium is likely to be the result of precipitation of an amorphous precursor in the presence of nanofibers with calcium binding phosphorylated or glutamic acid residues. The PA nanofibers used here with and without phosphorylated residues inherently favor the formation of hydroxyapatite in the culture medium used. To better understand the nucleation of hydroxyapatite on the PA nanofibers, PA gels were embedded and cross-sectioned for imaging by TEM. Figure 6 shows S(P) PA after 24 hours of mineralization (A), and then stained with uranyl acetate (UA) after 24 hours (B). Comparing Figures 6A and 6B, it is clear that the contrast of the mineral associated with the PA nanofibers is not an artifact of the UA stain. It is also clear that the mineral is directly associated with the PA nanofibers, suggesting the mineral does not precipitate from solution and instead the nanofibers are directly associated with the formation of hydroxyapatite. One can infer from these observations that the nanofibers nucleate the transformation of the spherical amorphous precursor particles to agglomerates of hydroxyapatite crystals. Figure 7 illustrates the templated mineral on each of the four PA gel mixtures mineralized for 24 hours (left) and 72 hours (right) with UA staining. It is clear from these images that nucleation of hydroxyapatite occurs on both S(P) and S PAs, with and without 5% RGDS PA. This confirms the findings by SEM, and shows that mineral is formed in the middle of the gel as well at the surface. While nano-scale, crystalline,

spherical calcium phosphate powders have been produced by methods including aqueous precipitation with sintering [24] and by sol-gel methods with sintering [25], we have demonstrated the ability to form crystalline hydroxyapatite on nanofibers without sintering. The mode of mineralization on PA nanofibers observed in this work in a calcium supplemented osteogenic medium is distinct from those reported previously by the authors' laboratory. First it is largely not epitaxial but yet it yields crystalline hydroxyapatite which based on the spheroidal shape appears to originate from an amorphous precursor. Secondly, in contrast to epitaxial mineralization reported previously, it is not affected by phosphorylation of serine residues of the PA. We infer the reason is the rapid precipitation of the amorphous precursor in the osteogenic medium for MSCs. At the same time, a common feature with epitaxial processes reported earlier is the direct involvement of the nanofibers in nucleating mineral formation.

3.2. Differentiation of hMSCs in Mineralizable Peptide Amphiphile Gels

We cultured human mesenchymal stem cells in the mineralizable gels to determine the effect of this environment on their differentiation. The effect of the four PA compositions, as well as the effect of pre-mineralized gels was evaluated. QRT-PCR was used to determine the gene expression of two osteogenic markers, alkaline phosphatase (ALP) and osteopontin (OP) after two and four weeks of culture. ALP is a glycoprotein enzyme that is involved in bone mineralization, although the control of its expression is not completely understood. Nevertheless, it is commonly used as an early indicator of osteoblastic differentiation [26]. OP, another glycoprotein originally found in bone matrix extracts, is expressed in high levels in the late stages of osteoblastic maturation, just prior to matrix mineralization [27]. Consequently, it is a good indicator of hMSC differentiation into mature osteoblasts. To confirm that the genes probed are actually produced by the cells, immunohistochemistry of ALP and OP are also presented. The results for cells cultured on the four PA mixtures are shown in Figure 8. The data indicate that the incorporation of phosphorylated serine leads to higher levels of ALP expression ($p<0.001$; PoT=0.991). The addition of the RGDS epitope did not inhibit this effect. Statistical differences between individual groups at a given time point or for a given PA formulation at different time points are indicated on the graph for ALP (Figure 8A). The data for OP gene expression demonstrates there is an effect of both phosphorylated serine ($p=0.001$; PoT=0.924) and RGDS epitope ($p=0.010$; PoT=0.658). This is primarily the result of the high OP expression observed at week 4 in the 100% serine PA formulation, which was significantly higher than every other formulation at week 4 and significantly higher than the same formulation at week 2 (Figure 8B). Given the expected late onset of OP expression, it is not surprising that there is no effect by week 2 for any of the formulations. The origin of this observation is not clear at the moment and could be associated with the fact that the role of OP in bone formation is very different from that of ALP. ALP is definitely required for mineral formation, but OP on the other hand appears to be associated with osteoclast function and bone remodeling and also inhibits mineral formation [28]. Combined, the data indicates that both PAs investigated direct the hMSCs toward the osteoblastic lineage. This is similar to the findings of Hosseinkhani et al., who observed increased ALP activity and osteocalcin content for rat MSCs cultured in RGD-containing peptide amphiphiles in an osteogenic medium up to 4 weeks [29].

To determine the effect of pre-mineralizing the PA nanofiber gels, hMSCs were seeded on top of fresh PA gels (termed S-on and S(P)-on, respectively) and two week pre-mineralized PA gels (termed pre-M S and pre-M S(P), respectively). After two and four weeks of culture, the cells were harvested and the ALP and OP gene expression was quantified by QRT-PCR, as shown in Figure 9. The data show that there is no overall effect of pre-mineralization on ALP or OP gene expression. As before, however, there is an overall statistical effect of phosphorylated serine elevating ALP gene expression and decreasing OP

gene expression. Statistical differences between individual groups at a given time point or for a given PA formulation at different time points are indicated on the graphs for ALP and OP (Figure 8A & B, respectively). Given the fast rate of mineral formation on the PA nanofibers (within 24 hours there is significant mineral) and relatively slow rate of differentiation of hMSCs in the PA gels (on the order of weeks for osteoblastic differentiation), the data indicates that the early influence of the mineral does not have a significant effect on the cells measured after two or four weeks.

Immunohistochemistry (IHC) was used to confirm that the genes for ALP and OP expressed resulted in protein production. Figure 10 shows representative images of cryo-sectioned PA gels containing hMSCs cultured for 4 weeks. The images clearly show the presence of both ALP (left panel) and OP (right panel). In addition to confirming the PCR data, the IHC validates the potential of these PA nanofiber systems for culturing hMSCs and inducing their differentiation toward the osteoblastic lineage.

Recently several groups have shown the osteoconductive [30] and osteoinductive [31–33] properties of calcium phosphate minerals and composites both *in vitro* and *in vivo*. In agreement with these findings, the early formation of hydroxyapatite that forms on our nanofiber networks under standard culture conditions for human mesenchymal stem cells as shown here suggests similar osteogenic activity. In future studies it will be interesting to establish a more comprehensive analysis of differentiation through additional markers and to control the *in vitro* environment to obtain specific modes of mineralization such as the one found here and the epitaxial mode identified previously by our group. Furthermore, an even greater challenge in future work is to establish which modes of mineralization occur *in vivo* and how they affect bone formation. In recent work from our laboratory [34], we showed that nanofibers containing S(P) residues lead to bone formation *in vivo* to an extent that is comparable to demineralized bone matrix, which was not the case for PAs containing S residues. It is not clear if this observation is related to the greater upregulation of ALP *in vitro* found in this work using nanofibers containing S(P) residues compared to systems containing non-phosphorylated S residues. An alternative explanation is that bone formation *in vivo* benefits from epitaxial biomimetic mineralization with S(P) nanofibers. In either case, we conclude that phosphorylated nanofibers are an important bioactive element in osteogenesis.

4. Conclusions

In calcium supplemented osteogenic media, peptide amphiphile nanofibers containing serine or phosphoserine residues nucleate on their surfaces spheroidal aggregates of carbonated hydroxyapatite crystals that appear to originate from an amorphous precursor. RGDS-bearing PA that may promote cell adhesion can be mixed in at 5% by weight without inhibiting this type of mineral formation. The mineralized nanofibers appear to promote osteogenic differentiation of mesenchymal stem cells based on alkaline phosphatase and osteopontin expression, a process that is possibly enhanced by the presence of phosphoserine residues in the peptide sequence.

Acknowledgments

The authors gratefully acknowledge funding support from the National Institutes of Health-National Institute of Dental and Craniofacial Research under award no. 5R01DE015920. Electron microscopy was performed in the Electron Probe Instrumentation Center (EPIC) facility of the NUANCE Center at Northwestern University, and is supported by NSF-NSEC, NSF-MRSEC, Keck Foundation, the State of Illinois, and Northwestern University; electron microscopy was also performed in the Biological Imaging Facility (BIF) at Northwestern University, and is supported by Weinberg College of Arts and Sciences, the Department of Neurobiology and Physiology, the Department of Biochemistry, Molecular Biology, and Cell Biology, the Robert H. Lurie Comprehensive Cancer Center and the Rice Foundation. Cell work was performed in the Institute for BioNanotechnology in Medicine

(IBNAM) at Northwestern University. We thank Dr. Shuyou Li and Mr. Ben Myers for their technical help with experiments at EPIC, Dr. William Russin and Ms. Ramona Walsh for their technical help with experiments at BIF, and Dr. Ramille Shah, Dr. Shuming Zhang, and Ms. Janet Martinez for their technical help with experiments at IBNAM. Conrado Aparicio would also like to thank the Generalitat de Catalunya for stipend support during his stay Northwestern University.

References

1. Long, PK.; Ibrahim, S. Autogenous Bone Grafting in Orthopaedic Surgery. In: Nather, A., editor. Bone grafts and bone substitutes : basic science and clinical applications. Hackensack, N.J: World Scientific; 2005. p. xviip. 592
2. Finkemeier CG. Bone-Grafting and Bone-Graft Substitutes. J Bone Joint Surg Am. 2002 Mar 1; 84(3):454–464. [PubMed: 11886919]
3. Cuomo AV, Virk M, Petrigliano F, Morgan EF, Lieberman JR. Mesenchymal Stem Cell Concentration and Bone Repair: Potential Pitfalls from Bench to Bedside. J Bone Joint Surg Am. 2009 May 1; 91(5):1073–1083. [PubMed: 19411455]
4. Vikram, D.; Nather, A.; Khalid, KA. Role of Ceramics as Bone Graft Substitutes. In: Nather, A., editor. Bone grafts and bone substitutes : basic science and clinical applications. Hackensack, N.J: World Scientific; 2005. p. xviip. 592
5. Palmer LC, Newcomb CJ, Kaltz SR, Spoerke ED, Stupp SI. Biomimetic Systems for Hydroxyapatite Mineralization Inspired By Bone and Enamel. Chemical Reviews. 2008; 108(11): 4754–4783. [PubMed: 19006400]
6. Hwang JJ, Jaeger K, Hancock J, Stupp SI. Organoapatite growth on an orthopedic alloy surface. Journal of Biomedical Materials Research. 1999; 47(4):504–515. [PubMed: 10497285]
7. Müller-Mai CM, Stupp SI, Voigt C, Gross U. Nanoapatite and organoapatite implants in bone: Histology and ultrastructure of the interface. Journal of Biomedical Materials Research. 1995; 29(1):9–18. [PubMed: 7713964]
8. Stupp SI, Ciegler GW. Organoapatites: Materials for artificial bone. I. Synthesis and microstructure. Journal of Biomedical Materials Research. 1992; 26(2):169–183. [PubMed: 1569112]
9. Spoerke ED, Stupp SI. Colonization of organoapatite-titanium mesh by preosteoblastic cells. Journal of Biomedical Materials Research Part A. 2003; 67A(3):960–969. [PubMed: 14613245]
10. Stupp SI, Hanson JA, Eurell JA, Ciegler GW, Johnson A. Organoapatites: Materials for artificial bone. III. Biological testing. Journal of Biomedical Materials Research. 1993; 27(3):301–311. [PubMed: 8360200]
11. Hartgerink JD, Beniash E, Stupp SI. Self-assembly and mineralization of peptide-amphiphile nanofibers. Science. 2001 Nov 23; 294(5547):1684–1688. [PubMed: 11721046]
12. Spoerke ED, Anthony SG, Stupp SI. Enzyme Directed Templating of Artificial Bone Mineral. Advanced Materials. 2009; 21(4):425–430. [PubMed: 22068437]
13. Sargeant TD, Guler MO, Oppenheimer SM, Mata A, Satcher RL, Dunand DC, et al. Hybrid bone implants: Self-assembly of peptide amphiphile nanofibers within porous titanium. Biomaterials. 2008 Jan; 29(2):161–171. [PubMed: 17936353]
14. Sargeant TD, Rao MS, Koh C-Y, Stupp SI. Covalent functionalization of NiTi surfaces with bioactive peptide amphiphile nanofibers. Biomaterials. 2008; 29(8):1085–1098. [PubMed: 18083225]
15. Sargeant TD, Oppenheimer SM, Dunand DC, Stupp SI. Titanium foam-bioactive nanofiber hybrids for bone regeneration. Journal of Tissue Engineering and Regenerative Medicine. 2008; 2(8):455–462. [PubMed: 18850672]
16. Lees, S. Some characteristics of mineralised collagen. In: Hukins, DWL., editor. Calcified tissue. Boca Raton, Fla: CRC Press; 1989. p. xip. 250
17. Rexeisen EL, Fan W, Pangburn TO, Taribagil RR, Bates FS, Lodge TP, et al. Self-Assembly of Fibronectin Mimetic Peptide-Amphiphile Nanofibers. Langmuir. 2009; 26(3):1953–1959. [PubMed: 19877715]
18. Galler KM, Cavender A, Yuwono V, Dong H, Shi S, Schmalz G, et al. Self-Assembling Peptide Amphiphile Nanofibers as a Scaffold for Dental Stem Cells. Tissue Engineering Part A. 2008; 14(12):2051–2058. 2011/09/14. [PubMed: 18636949]

19. Guler MO, Hsu L, Soukasene S, Harrington DA, Hulvat JF, Stupp SI. Presentation of RGDS epitopes on self-assembled nanofibers of branched peptide amphiphiles. Biomacromolecules. 2006 Jun; 7(6):1855–1863. [PubMed: 16768407]
20. Guler MO, Soukasene S, Hulvat JF, Stupp SI. Presentation and recognition of biotin on nanofibers formed by branched peptide amphiphiles. Nano Lett. 2005 Feb; 5(2):249–252. [PubMed: 15794605]
21. LeGeros, RZ. Calcium phosphates in oral biology and medicine. Basel New York: Karger; 1991.
22. Rey C, Combes C, Drouet C, Sfihi H, Barroug A. Physico-chemical properties of nanocrystalline apatites: Implications for biominerals and biomaterials. Materials Science & Engineering C-Biomimetic and Supramolecular Systems. 2007 Mar; 27(2):198–205.
23. Mahamid J, Sharir A, Addadi L, Weiner S. Amorphous calcium phosphate is a major component of the forming fin bones of zebrafish: Indications for an amorphous precursor phase. Proceedings of the National Academy of Sciences. 2008 Sep 2; 105(35):12748–12753.
24. Zhao Y, Zhang Y, Ning F, Guo D, Xu Z. Synthesis and cellular biocompatibility of two kinds of HAP with different nanocrystal morphology. Journal of Biomedical Materials Research Part B-Applied Biomaterials. 2007 Oct; 83B(1):121–126.
25. Fathi MH, Hanifi A. Evaluation and characterization of nanostructure hydroxyapatite powder prepared by simple sol-gel method. Materials Letters. 2007 Jul; 61(18):3978–3983.
26. Henthorn, PS. Alkaline Phosphatase. In: Bilezikian, JP.; Raisz, LG.; Rodan, GA., editors. Principles of bone biology. San Diego: Academic Press; 1996. p. xxp. 1398
27. Robey, PG. Bone Matrix Proteoglycans and Glycoproteins. In: Bilezikian, JP.; Raisz, LG.; Rodan, GA., editors. Principles of bone biology. San Diego: Academic Press; 1996. p. xxp. 1398
28. Standal T, Borset M, Sundan A. Role of osteopontin in adhesion, migration, cell survival and bone remodeling. Exp Oncol. 2004 Sep; 26(3):179–184. [PubMed: 15494684]
29. Hosseinkhani H, Hosseinkhani M, Tian F, Kobayashi H, Tabata Y. Osteogenic differentiation of mesenchymal stem cells in self-assembled peptide-amphiphile nanofibers. Biomaterials. 2006; 27(22):4079–4086. [PubMed: 16600365]
30. Müller P, Bulnheim U, Diener A, Lüthen F, Teller M, Klinkenberg E-D, et al. Calcium phosphate surfaces promote osteogenic differentiation of mesenchymal stem cells. Journal of Cellular and Molecular Medicine. 2008; 12(1):281–291. [PubMed: 18366455]
31. Narducci P, Nicolin V. Differentiation of activated monocytes into osteoclast-like cells on a hydroxyapatite substrate: an in vitro study. Annals of Anatomy-Anatomischer Anzeiger. 2009; 191(4):349–355.
32. Osathanon T, Linnes ML, Rajachar RM, Ratner BD, Somerman MJ, Giachelli CM. Microporous nanofibrous fibrin-based scaffolds for bone tissue engineering. Biomaterials. 2008; 29(30):4091–4099. [PubMed: 18640716]
33. Kim SE, Choi HW, Lee HJ, Chang JH, Choi J, Kim KJ, et al. Designing a highly bioactive 3D bone-regenerative scaffold by surface immobilization of nano-hydroxyapatite. Journal of Materials Chemistry. 2008; 18(41):4994–5001.
34. Mata A, Geng Y, Henrikson KJ, Aparicio C, Stock SR, Satcher RL, Stupp SI. Bone regeneration mediated by biomimetic mineralization of a nanofiber matrix. Biomaterials. 2010; 31(23):6004–6012. [PubMed: 20472286]

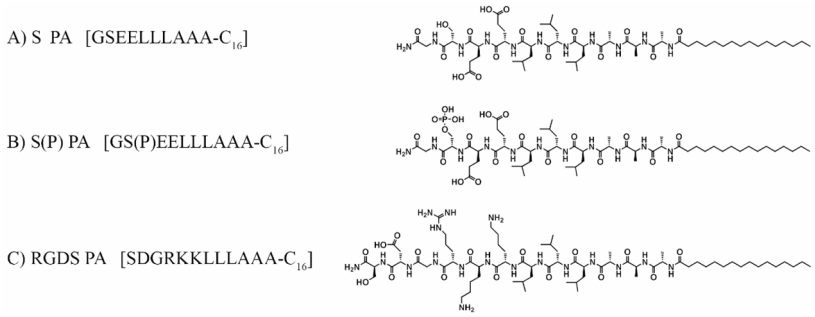

Figure 1.
Chemical structures of the 3 PAs used to create nanofiber gels: A) net negatively charged serine-bearing PA, B) net negatively charged phosphoserine-bearing PA, and C) net positively charged RGDS-bearing PA.

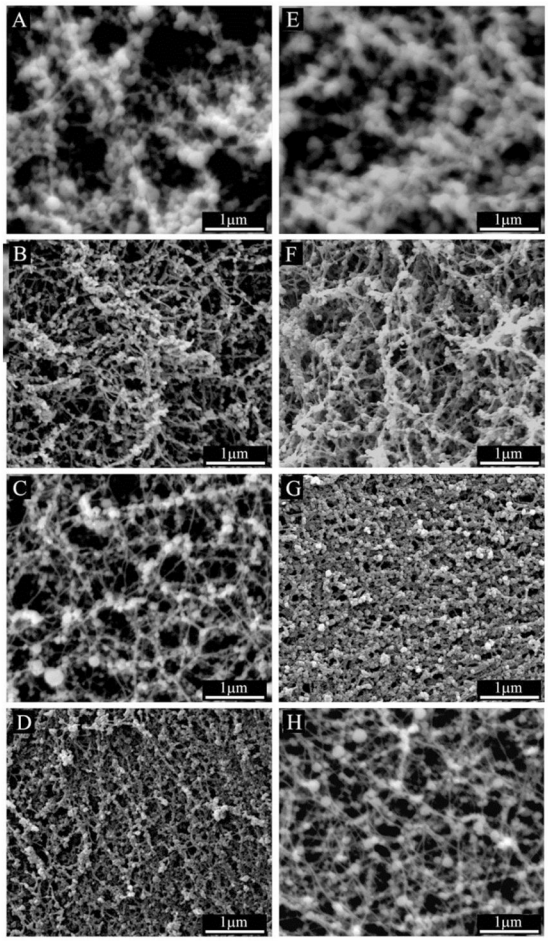

Figure 2.
SEM images of 10 mM PA gels mineralized for 3 days (left column) and 7 days (right column) in hMSC osteogenic medium supplemented with 20 mM $CaCl_2$ (mineralization medium). From top to bottom, 100% S PA (A, E), 95% S/5% RGDS PA (B, F), 100% S(P) PA (C, G), and 95% S(P)/5% RGDS PA (D, H). All PAs show the formation of spherical nodules of calcium phosphate mineral associated with the PA nanofibers.

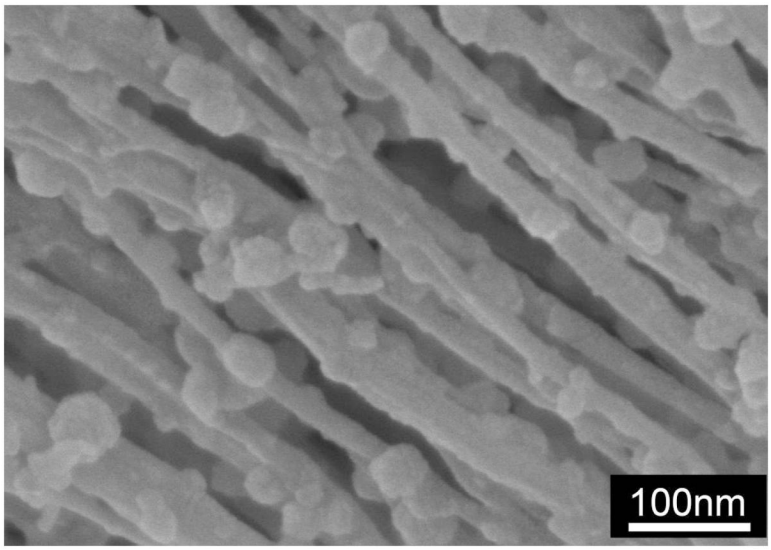

Figure 3.
High resolution SEM image of mineralized PA nanofibers. The PA has the amino acid sequence GS(P)EEAAAVVV-C_{16} and was mineralized under the same conditions as the other PAs used here. The spheroidal mineral nodules can be clearly seen nucleated on the nanofibers.

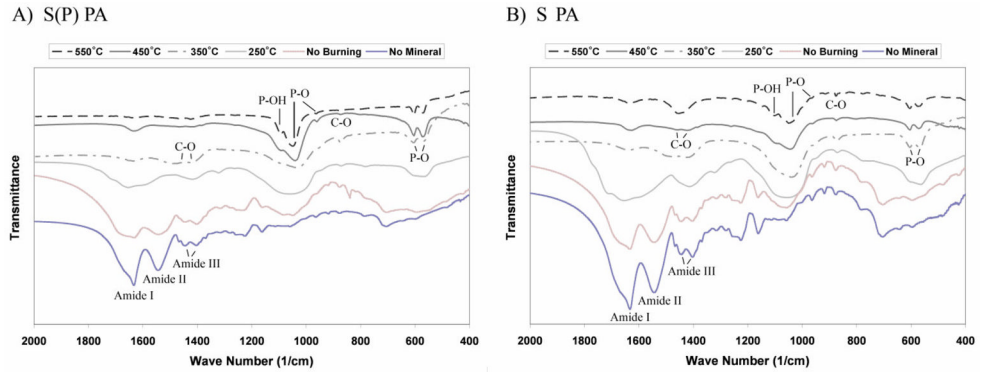

Figure 4.

FT-IR spectra of S(P) PA (A) and S PA (B) mineralized for 2 weeks in hMSC osteogenic medium supplemented with 20 mM $CaCl_2$ (mineralization culture medium). Mineralized PA gels were washed to remove medium components and then burned at various temperatures to remove the PA, leaving behind only mineral. Peaks that correspond to the PA (Amide I, II, III) and carbonated hydroxyapatite (C-O, P-O, and P-OH) are indicated.

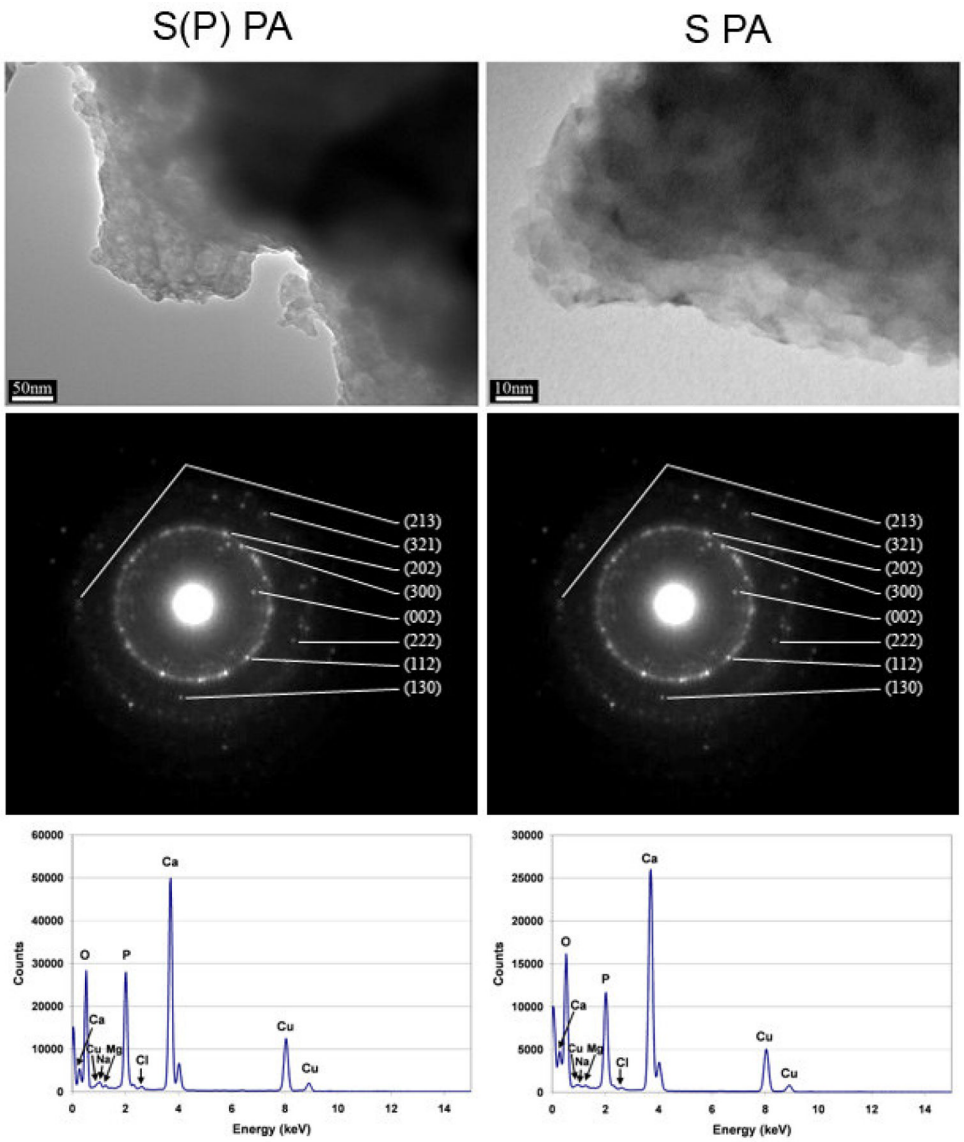

Figure 5.

TEM images, diffraction patterns, and EDS spectra from mineralized S(P) PA (left) and S PA (right) after washing and burning at 350°C to remove residual medium components and the PA. The remaining mineral from both PAs each produce a diffraction pattern corresponding to hydroxyapatite.

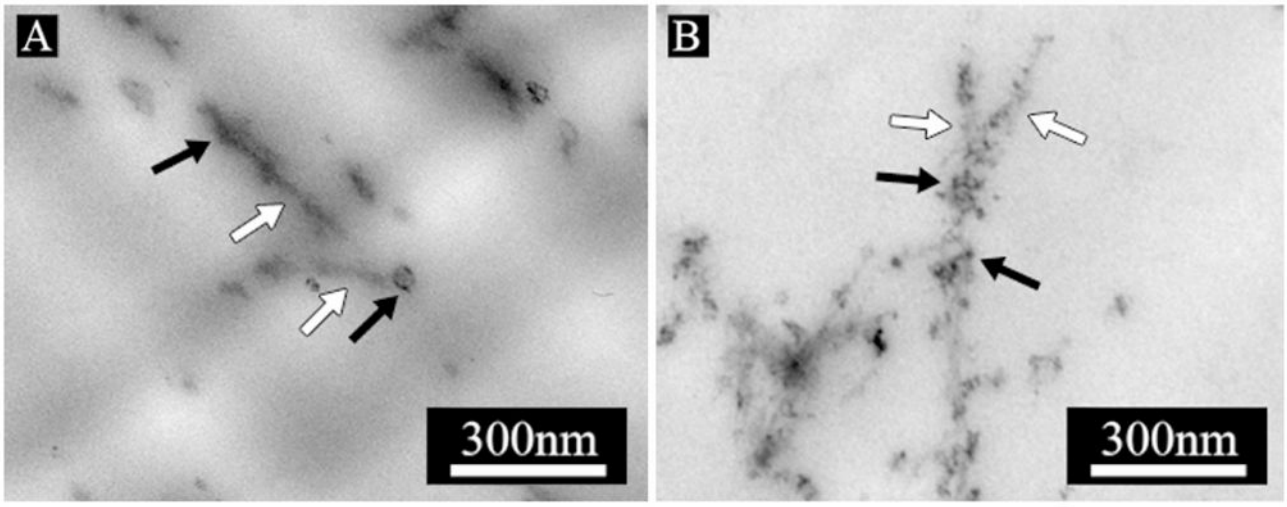

Figure 6.
TEM images of embedded and cross-sectioned 10 mM S(P) PA gels mineralized in hMSC osteogenic medium supplemented with 20 mM $CaCl_2$ (mineralization culture medium). From left to right: S(P) PA mineralized for 24 hours with no stain (A), and S(P) PA mineralized for 24 hours with UA stain (B). PA nanofibers are indicated with white arrows, mineral is indicated with black arrows.

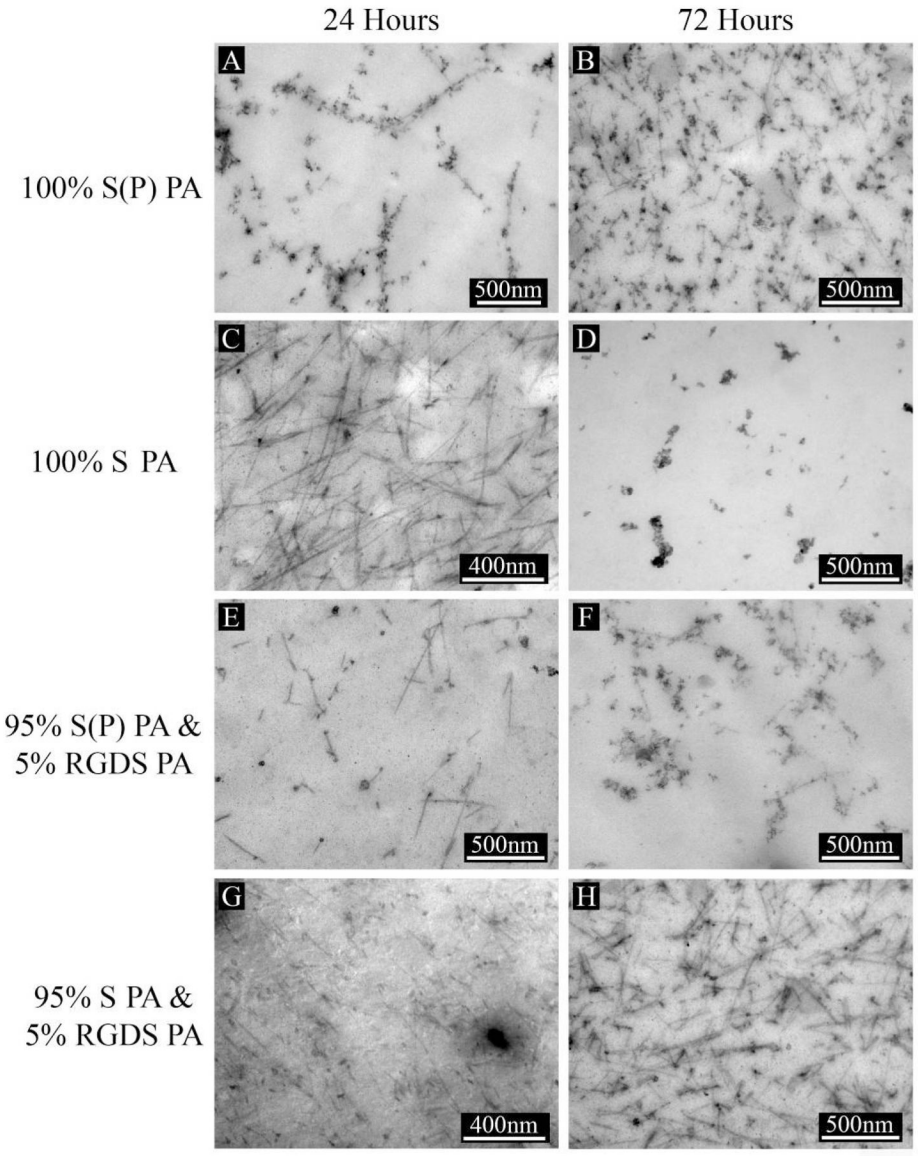

Figure 7.

TEM images of embedded and cross-sectioned 10 mM PA gels mineralized for 24 hours (left column) and 72 hours (right column) in hMSC osteogenic medium supplemented with 20 mM $CaCl_2$ (mineralization culture medium). Images shown are representative of 100% S(P) PA gels (A, B), 100% S PA gels (C, D), 95% S(P) & 5% RGDS PA gels (E, F), and 95% S & 5% RGDS PA gels (G, H). All PAs show the formation of mineral along the nanofibers.

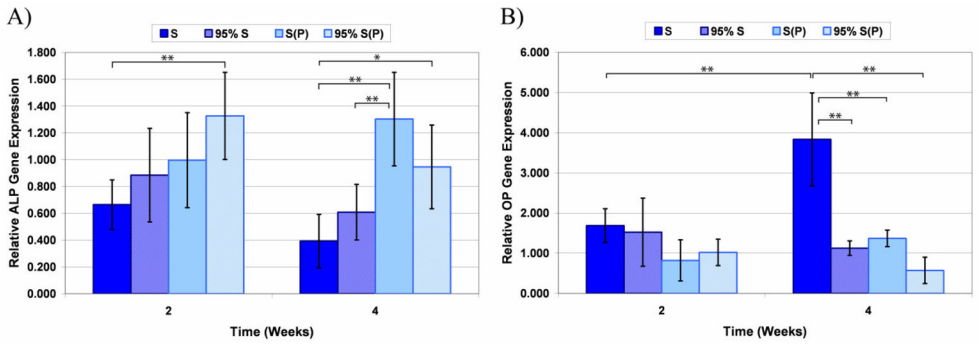

Figure 8.

QRT-PCR data for hMSCs cultured in 100% S PA, 95% S/5% RGDS PA, 100% S(P) PA, and 95% S(P)/5% RGDS PA. Samples were assayed for alkaline phosphatase (ALP) gene expression (A) and osteopontin (OP) gene expression (B). Significant differences are indicated as *$p<0.05$ and **$p<0.01$.

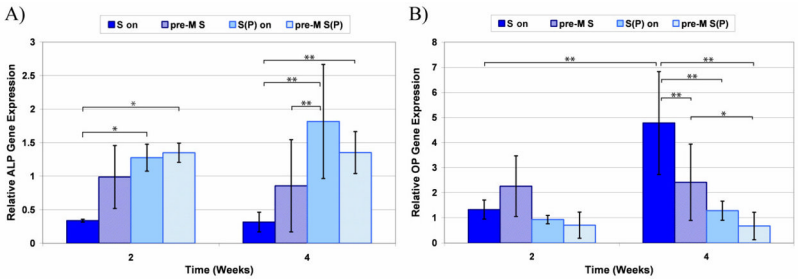

Figure 9.

QRT-PCR data for hMSCs cultured on 100% S PA or 100% S(P) PA gels that were pre-mineralized (termed pre-M S and pre-M S(P), respectively) or not (termed S-on and S(P)-on, respectively). Samples were assayed for alkaline phosphatase (ALP) gene expression (A) and osteopontin (OP) gene expression (B). Significant differences are indicated as *$p<0.05$ and **$p<0.01$.